

000 001 REINFORCEMENT LEARNING FINE-TUNING EN- 002 HANCES ACTIVATION INTENSITY AND DIVERSITY 003 IN THE INTERNAL CIRCUITRY OF LLMs 004 005

006 **Anonymous authors**
007 Paper under double-blind review
008
009
010
011
012

ABSTRACT

013 Large language models (LLMs) acquire extensive prior knowledge through large-
014 scale pretraining and can be further enhanced via supervised fine-tuning (SFT)
015 or reinforcement learning (RL)-based post-training. A growing body of evidence
016 has shown that RL fine-tuning improves the capability of LLMs beyond what SFT
017 alone achieves. However, the underlying mechanisms why RL fine-tuning is able
018 to enhance the capability of various LLMs with distinct intrinsic characteristics
019 remain underexplored. In this study, we draw inspiration from prior work on edge
020 attribution patching (EAP) to investigate the internal differences of LLMs before
021 and after RL fine-tuning. Our analysis across multiple model families and mathe-
022 matical datasets shows two robust effects of online RL post-training: (*i*) an overall
023 increase in average activation intensity, indicating that more internal pathways are
024 engaged and their signals become stronger, and (*ii*) greater diversity in activa-
025 tion patterns, reflected by higher entropy and less concentrated edge distributions.
026 These changes suggest that RL reshapes information flow to be both more redun-
027 dant and more flexible, which may explain its advantage in mathematical gener-
028 alization. Notably, models fine-tuned with Direct Preference Optimization (DPO)
029 deviate from these trends, exhibiting substantially weaker or inconsistent internal
030 changes compared to PPO- and GRPO-based training. Together, our findings
031 provide a unified view of how RL fine-tuning systematically alters the internal cir-
032 cuity of LLMs and highlight the methodological distinctions between online RL
033 and preference-based approaches. Our code is open source at https://anonymous.4open.science/r/llm_rl_probing_analysis-F673.
034

1 INTRODUCTION

035 Recent strides in large language models (LLMs) have shifted the developmental focus from pre-
036 training to post-training (Kumar et al., 2025). A wide array of post-training strategies, ranging
037 from supervised fine-tuning (SFT) (Dong et al., 2023) to reinforcement learning (RL) (Zhang et al.,
038 2025b; Hao et al., 2025), has been developed to enhance model performance. Particularly, RL-based
039 fine-tuning has witnessed rapid advancements, encompassing the development of reward models
040 from Outcome Reward Models (ORM) (Lyu et al., 2025) to Process Reward Models (PRM) (Light-
041 man et al., 2023; Yuan et al., 2024), alongside training algorithms like Proximal Policy Optimiza-
042 tion (PPO) (Schulman et al., 2017) and Group Relative Policy Optimization (GRPO) (Shao et al.,
043 2024). With such advancements, emerging empirical evidence indicates that RL-based fine-tuning
044 can enhance the capability of LLMs beyond what is achieved by SFT alone (Chu et al., 2025),
045 improving performance across a range of downstream tasks, including writing (Liao et al., 2025),
046 reasoning (Guo et al., 2025; Xu et al., 2025), and coding (Guo et al., 2024).
047

048 Seeking to understand the role of different components within Large Language Models (LLMs)
049 and the origins of their powerful capabilities, a growing body of research has focused on probing
050 their internal structures. Initial studies revealed the working mechanisms of LLMs when solving
051 mathematical problems by analyzing and statistically examining their internal weights (Shao et al.,
052 2025). Subsequently, some research has analyzed patterns in LLM weights by training external
053 neural probes, which are lightweight auxiliary models (Kim et al., 2025; Zheng et al., 2025). Re-
cently, researchers have investigated the internal residual pathways of LLMs from a graph-theoretic

perspective. They have developed methods such as Automated Circuit Discovery (ACDC) (Conmy et al., 2023) and Edge Attribution Patching (EAP) (Syed et al., 2023; Hanna et al., 2024), which assign importance scores to edges or sub-modules and reveal internal functional circuits that determine the capabilities of LLMs.

Despite these advances, existing studies on RL-based post-training have predominantly focused on the external behavioral changes of LLMs, while the underlying internal mechanisms remain under-explored (Ren & Sutherland, 2024). Conversely, works that do investigate the internal mechanisms concentrate on given LLMs, but do not correlate the internal mechanisms to the RL-based post-training methodology with which the LLMs are commonly obtained (Hanna et al., 2024; Kim et al., 2025). As a result, the two lines of research, external evaluation of RL effects and internal mechanistic analysis, have largely progressed in parallel. This gap is partly due to the primary goal of RL post-training, namely enhancing the ability of LLMs to solve complex reasoning tasks, which makes it nontrivial to directly transfer analytical strategies developed on toy problems to the study of RL-induced improvements in real-world problem-solving capabilities.

To address this, we construct a framework for systematically analyzing the mechanisms through which RL fine-tuning affects LLMs. Specifically, we adopt an efficient Edge Attribution Patching (EAP) framework (Nanda, 2023), leveraging the cross-entropy computed from partially truncated generations on mathematical problem-solving tasks to estimate the contribution weights of internal edges. Based on these estimated importance weights, we analyze their distributions before and after RL fine-tuning to interpret changes in internal neuron activations and derive general conclusions regarding the structural effects of RL in the context of mathematical problem solving. Experiments across multiple LLM pairs on diverse mathematical datasets demonstrate that RL post-training strengthens the activation intensity of internal edge connections and diversifies activation patterns during problem-solving. Notably, these effects are not consistently observed under DPO training, highlighting differences between DPO and other RL paradigms, which aligns with prior observations in the literature (Xu et al., 2024).

Overall, the uncovered patterns hold across diverse LLM families, each with distinct characteristics such as architecture and training corpus, suggesting a set of common internal effects induced by RL fine-tuning on reasoning-heavy tasks. These findings provide new insights into how RL post-training reshapes the internal circuitry of LLMs, thereby bridging empirical performance gains with interpretable shifts in internal information pathways. In doing so, they offer guidance for the future development of both LLMs and post-training methodologies.

2 PRELIMINARIES

2.1 LARGE LANGUAGE MODELS

Large language models (LLMs) are typically built upon the Transformer architecture, comprising a stack of L identical layers (Vaswani et al., 2017; Liu et al., 2024; Bai et al., 2023; Achiam et al., 2023). Each layer consists of two primary sub-structures: a multi-head self-attention mechanism and a position-wise feed-forward network (FFN), each surrounded by a residual connection. The mathematical formulation described below represents the most common architecture found in contemporary LLMs. Let $\mathbf{H}^{(2\ell)} \in \mathbb{R}^{B \times P \times d_{\text{model}}}$ denote the input hidden state to the $(\ell + 1)$ -th layer, where B is the batch size, P is the sequence length, and d_{model} is the hidden dimension. Specifically, the raw input embeddings are denoted by $\mathbf{X}_{\text{input}} = \mathbf{H}^{(0)}$.

The output of the ℓ -th layer, $\mathbf{H}^{(2\ell)}$, is computed via the sequential processing of the attention and FFN sub-structures. For the attention sub-structure, the input is first normalized as $\mathbf{X}_{\text{attn}}^\ell = \text{LayerNorm}(\mathbf{H}^{(2\ell-2)})$. The attention mechanism is then applied:

$$\text{Attention}(\mathbf{X}_{\text{attn}}^\ell) = \mathbf{O}_{\text{attn}}^\ell = \text{softmax} \left(\frac{(\mathbf{X}_{\text{attn}}^\ell \mathbf{W}_q^\ell) (\mathbf{X}_{\text{attn}}^\ell \mathbf{W}_k^\ell)^T}{\sqrt{d_k}} \right) (\mathbf{X}_{\text{attn}}^\ell \mathbf{W}_v^\ell) \mathbf{W}_o^\ell, \quad (1)$$

where $\mathbf{W}_q^\ell, \mathbf{W}_k^\ell \in \mathbb{R}^{d_{\text{model}} \times d_{\text{query}}}$, $\mathbf{W}_v^\ell \in \mathbb{R}^{d_{\text{model}} \times d_{\text{attn}}}$, $\mathbf{W}_o^\ell \in \mathbb{R}^{d_{\text{attn}} \times d_{\text{model}}}$ are the query, key, value and output projection matrices, respectively. Here, d_{query} is the dimensionality of the query and key vectors, and d_{attn} represents the dimensionality of the value vectors within the attention computation.

108 Positional embeddings are omitted for simplicity. The residual connection yields the intermediate
 109 state: $\mathbf{H}^{(2\ell-1)} = \mathbf{H}^{(2\ell-2)} + \mathbf{O}_{\text{attn}}^\ell$.
 110

111 The FFN sub-structure then processes $\mathbf{H}^{(2\ell-1)}$ after normalization: $\mathbf{X}_{\text{ffn}}^\ell = \text{LayerNorm}(\mathbf{H}^{(2\ell)})$.
 112 The FFN employs a gated mechanism with parallel pathways:

$$\text{FFN}(\mathbf{X}_{\text{ffn}}^\ell) = \mathbf{O}_{\text{ffn}}^\ell = (\text{Activation}(\mathbf{X}_{\text{ffn}}^\ell \mathbf{W}_{\text{gate}}^\ell) \odot (\mathbf{X}_{\text{ffn}}^\ell \mathbf{W}_{\text{up}}^\ell)) \mathbf{W}_{\text{down}}^\ell, \quad (2)$$

113 where $\mathbf{W}_{\text{gate}}^\ell \in \mathbb{R}^{d_{\text{model}} \times d_{\text{ff}}}$, $\mathbf{W}_{\text{up}}^\ell \in \mathbb{R}^{d_{\text{model}} \times d_{\text{ff}}}$, and $\mathbf{W}_{\text{down}}^\ell \in \mathbb{R}^{d_{\text{ff}} \times d_{\text{model}}}$ are learned weight matrices,
 114 \odot denotes element-wise multiplication, and d_{ff} is the expanded inner dimension of the FFN. The
 115 final output of the layer is obtained via another residual connection: $\mathbf{H}^{(2\ell)} = \mathbf{H}^{(2\ell-1)} + \mathbf{O}_{\text{ffn}}^\ell$.
 116

117 After processing by all L layers, the final hidden states $\mathbf{H}^{(2L)}$ are projected to vocabulary logits via:
 118

$$\mathbf{L} = \mathbf{P}(\mathbf{H}^{(2L)}) = \text{LayerNorm}(\mathbf{H}^{(2L)}) \mathbf{W}_{\text{emb}}^T, \quad (3)$$

119 where $\mathbf{W}_{\text{emb}} \in \mathbb{R}^{V \times d_{\text{model}}}$ is the output embedding matrix and V is the vocabulary size. The resulting
 120 tensor $\mathbf{L} \in \mathbb{R}^{B \times P \times V}$ contains the unnormalized logits for each token position.
 121

2.2 UNIFIED VIEW OF LLM POST-TRAINING

122 Previous studies have shown that various post-training methods can be expressed within a unified
 123 framework (Shao et al., 2024), encompassing both supervised fine-tuning (SFT) and reinforcement
 124 learning (RL)-based approaches. Let π_θ denote the current policy parameterized by θ , and let (q, o)
 125 represent a query-response pair. The update rule of a generic post-training algorithm \mathcal{A} can then be
 126 written in gradient form as
 127

$$\nabla_\theta \mathcal{J}_{\mathcal{A}}(\theta) = \mathbb{E}_{(q, o) \sim \mathcal{D}} \left[\frac{1}{|o|} \sum_{t=1}^{|o|} GC_{\mathcal{A}}(q, o, t, \pi_{\text{rd}}, \pi_{\text{ref}}, \pi_\theta) \nabla_\theta \log \pi_\theta(o_t \mid q, o_{<t}) \right], \quad (4)$$

128 where \mathcal{D} specifies the sampling distribution that generates the training pairs (q, o) , π_{rd} denotes the
 129 reward model or evaluation rule that produces the learning signal, π_{ref} is the reference policy used to
 130 anchor relative preference or advantage computations, and $GC_{\mathcal{A}}$ represents the token-level weighting
 131 factor derived from these signals in algorithm \mathcal{A} . This abstraction places different post-training
 132 approaches within a unified mathematical representation, enabling direct comparison between su-
 133 pervised and reinforcement-driven update mechanisms.
 134

3 METHOD

135 Our methodology is based on the *Edge Attribution Patching* (EAP) framework (Syed et al., 2023;
 136 Hanna et al., 2024; Nanda, 2023), which adopts a graph-theoretic view of LLMs via their residual
 137 pathways, reflecting a perspective that has long been present in prior research. While the original
 138 work focuses on automated circuit discovery, we adapt its core principle of deriving gradient-based
 139 attribution scores for edges to analyze internal information flow differences between models before
 140 and after reinforcement learning (RL) fine-tuning.
 141

3.1 GRAPH VIEW OF TRANSFORMER RESIDUAL COMPUTATION

142 Owing to the residual connections in Transformer layers, the input to any sub-module, whether an
 143 attention branch or an FFN branch, corresponds to the sum of all preceding sub-module outputs,
 144 including the original embedding input. For simplicity, let the attention branch transformation be
 145 denoted as $\mathbf{O}_{\text{attn}}^\ell = \mathbf{A}^\ell(\mathbf{H}^{(2\ell)})$ and the FFN transformation as $\mathbf{O}_{\text{ffn}}^\ell = \mathbf{F}^\ell(\mathbf{H}^{(2\ell+1)})$. Then the
 146 hidden states satisfy:
 147

$$\mathbf{H}^{(2\ell)} = \mathbf{H}^{(0)} + \sum_{i=1}^{\ell} \mathbf{O}_{\text{attn}}^i + \sum_{j=1}^{\ell} \mathbf{O}_{\text{ffn}}^j, \quad \mathbf{H}^{(2\ell+1)} = \mathbf{H}^{(0)} + \sum_{i=1}^{\ell+1} \mathbf{O}_{\text{attn}}^i + \sum_{j=1}^{\ell} \mathbf{O}_{\text{ffn}}^j. \quad (5)$$

148 Consequently, each sub-module, namely any attention block \mathbf{A}^ℓ or feed-forward block \mathbf{F}^ℓ , can be
 149 interpreted as a node in a directed graph. Let us define the set of nodes as
 150

$$\mathcal{V} = \{\mathbf{A}^1, \mathbf{F}^1, \mathbf{A}^2, \mathbf{F}^2, \dots, \mathbf{A}^L, \mathbf{F}^L\}, \quad (6)$$

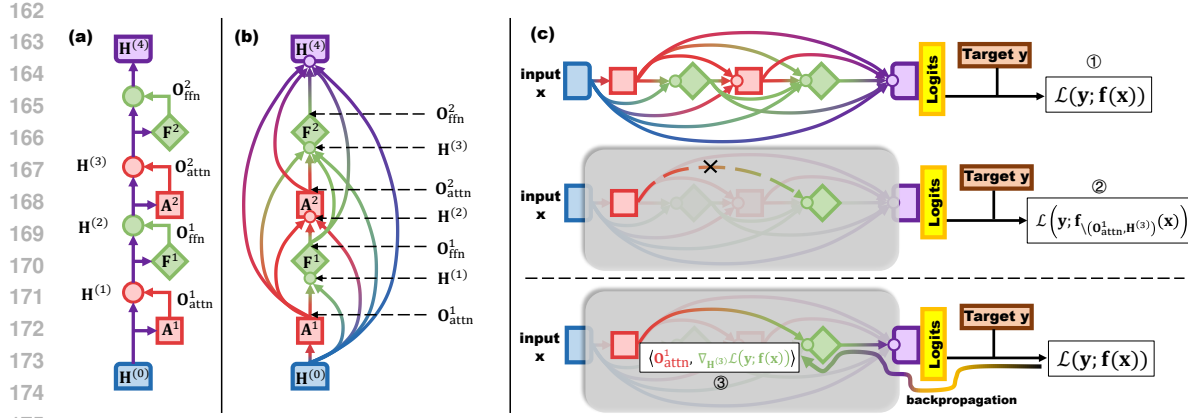


Figure 1: Schematic of a two-layer simplified LLM. (a) Residual perspective, (b) graph perspective, and (c) edge importance estimation: above the dashed line, ACDC-style methods measure the loss change after edge ablation (② – ①), and below, EAP-style methods approximate this via backpropagated gradients (–③) \approx (② – ①).

where \mathbf{H}^0 corresponds to the original embedding input. The directed edges, representing the flow of information from sub-module outputs to subsequent inputs, can be formalized as

$$\mathcal{E} = \left\{ \left(\mathbf{H}^{(0)}, \mathbf{H}^{(j)} \right) \mid 1 \leq j \leq 2L \right\} \cup \left\{ \left(\mathbf{O}_{\text{attn}}^i, \mathbf{H}^{(2\ell-1)} \right), \left(\mathbf{O}_{\text{ffn}}^i, \mathbf{H}^{(2\ell)} \right) \mid 1 \leq i \leq \ell \leq L \right\}. \quad (7)$$

Thus, the LLM can be represented as a directed acyclic graph (DAG) $\mathcal{G} = (\mathcal{V}, \mathcal{E})$, in which nodes correspond to individual sub-modules and edges encode the residual information pathways. This graph-theoretic abstraction facilitates analysis of the model both from a network flow perspective and a circuit-based interpretability standpoint, and for a more intuitive comparison of the residual stream view and the graph view, see Fig. 1(a) and (b).

3.2 EDGE-LEVEL ATTRIBUTION

To quantify the importance of individual residual edges, prior work like the *Automated Circuit Discovery* (ACDC) evaluates the change in loss when a given edge is removed (Conmy et al., 2023). Concretely, let $(\mathbf{O}, \mathbf{H}) \in \mathcal{E}$ denote a directed edge from output \mathbf{O} of some sub-module to hidden representation \mathbf{H} at a subsequent stage. ACDC defines the edge importance by the loss perturbation:

$$I_{\text{ACDC}}(\mathbf{O}, \mathbf{H}) = \mathcal{L}(\mathbf{y}; \mathbf{f}_{\setminus(\mathbf{O}, \mathbf{H})}(\mathbf{x})) - \mathcal{L}(\mathbf{y}; \mathbf{f}(\mathbf{x})), \quad (8)$$

where $\mathbf{f}(\mathbf{x})$ is the model output under input \mathbf{x} , $\mathcal{L}(\mathbf{y}; \cdot)$ denotes the supervised loss relative to target \mathbf{y} , and $\mathbf{f}_{\setminus(\mathbf{O}, \mathbf{H})}$ represents the model with edge (\mathbf{O}, \mathbf{H}) ablated (i.e., setting the corresponding contribution to zero). While conceptually straightforward, this procedure requires two forward passes per edge, rendering it computationally infeasible for large-scale attribution.

By contrast, the EAP framework proposes a gradient-based linearization that estimates the same loss perturbation more efficiently. Specifically, for a given edge (\mathbf{O}, \mathbf{H}) , consider the ablation $\mathbf{H} \mapsto \mathbf{H} - \mathbf{O}$, which corresponds to removing \mathbf{O} 's contribution. A first-order Taylor expansion around \mathbf{H} yields the following compact expression:

$$\Delta \mathcal{L}(\mathbf{O}, \mathbf{H}) \approx -\langle \nabla_{\mathbf{H}} \mathcal{L}(\mathbf{y}; \mathbf{f}(\mathbf{x})), \mathbf{O} \rangle \equiv I_{\text{EAP}}(\mathbf{O}, \mathbf{H}), \quad (9)$$

where $\nabla_{\mathbf{H}} \mathcal{L}(\mathbf{y}; \mathbf{f}(\mathbf{x})) \in \mathbb{R}^{B \times P \times d_{\text{model}}}$ is the loss gradient with respect to the hidden state \mathbf{H} , and $\langle \cdot, \cdot \rangle$ denotes the Euclidean inner product.

Considering the computational cost of analyzing large-scale LLMs, we adopt I_{EAP} to estimate edge-level importance. Importantly, I_{EAP} can be computed for all edges simultaneously with a single forward and backward pass under the zeroing perturbation, as both the forward activations \mathbf{O} and the backward gradients $\nabla_{\mathbf{H}} \mathcal{L}$ are available. This approach enables scalable, fine-grained circuit analysis without the need for separate per-edge ablations, making it tractable even for very large models. For a more intuitive comparison of ACDC-style ablation and EAP-style gradient-based attribution, see Fig. 1(c).

216
217

3.3 SAMPLE SELECTION AND TOKEN-LEVEL TRUNCATION

218
219
220
221
222

To ensure fair and tractable edge attribution analysis, we implement a systematic filtering and truncation procedure on model-generated token sequences. Let each model in a paired set generate a token sequence $\mathbf{s}^{\text{base}} = (s_1^{\text{base}}, \dots, s_{T_{\text{base}}}^{\text{base}})$ and $\mathbf{s}^{\text{RL}} = (s_1^{\text{RL}}, \dots, s_{T_{\text{RL}}}^{\text{RL}})$ for a given question, where T_{base}^q and T_{RL}^q are the respective sequence lengths.

223
224
225

Question Filtering. We first select only questions that are correctly answered by both models, and denote the resulting set as \mathcal{Q} . To mitigate biases caused by extremely short or long answers, we compute the mean token length across all selected questions for a given model pair and dataset:

226
227
228

$$\bar{T} = \frac{1}{|\mathcal{Q}|} \sum_{q \in \mathcal{Q}} \frac{T_{\text{base}}^q + T_{\text{RL}}^q}{2}. \quad (10)$$

229
230
231

We then define minimum and maximum allowable lengths, $T_{\min} = \beta \bar{T}$, $T_{\max} = \gamma \bar{T}$, and retain only questions satisfying

$$T_{\min} \leq T_{\text{base}}^q, T_{\text{RL}}^q \leq T_{\max}. \quad (11)$$

233
234

Finally, to control for comparable sequence lengths between the base and RL models, we require

235
236
237

$$\frac{|T_{\text{base}}^q - T_{\text{RL}}^q|}{(T_{\text{base}}^q + T_{\text{RL}}^q)/2} < \delta, \quad (12)$$

where $\delta \in (0, 1)$ is a balance coefficient. This ensures that the selected questions are comparable in length across both models, minimizing biases in edge importance estimates.

240
241
242
243
244
245

Token Truncation and Self-Entropy Computation. For the filtered set of questions, we define a truncation length $T_{\text{cut}} = \alpha \bar{T}$, where $\alpha > 0$ is a scaling coefficient. Only the first T_{cut} tokens of each sequence are used. Let $\mathbf{L}_t \in \mathbb{R}^V$ denote the model’s logit output at token position t , and let $\mathbf{s}_{1:T_{\text{cut}}}$ be the sequence of generated tokens truncated to T_{cut} . We compute the self-entropy (cross-entropy of the model with respect to its own output) as

246
247
248

$$\mathcal{L}_{\text{trunc}} = -\frac{1}{T_{\text{cut}}} \sum_{t=1}^{T_{\text{cut}}} \log \frac{\exp(\mathbf{L}_t[s_t])}{\sum_{v=1}^V \exp(\mathbf{L}_t[v])}, \quad (13)$$

249
250
251
252
253
254
255
256

where s_t denotes the token actually generated at position t by the model itself.

This ensures that edge importance is computed based on each model’s truncated output, maintaining comparability across sequences while avoiding excessive memory usage for overlong generations.

4 EXPERIMENT

257
258
259
260

4.1 EXPERIMENTAL SETTINGS

261
262
263
264
265

In our experiments, to ensure both reproducibility and the generality of the conclusions, we employed four pairs of open-source large language models (LLMs) of approximately 7B parameters, each consisting of a base model and its counterpart after post-training:

266
267
268
269

- **Deepseek-Math** (Shao et al., 2024): Both *deepseek-math-7b-instruct* and *deepseek-math-7b-rl* are official DeepSeek models based on the LLaMA-style Transformer. *deepseek-math-7b-instruct* is instruction-tuned on mathematical datasets such as GSM8K, MATH, and MathInstruct, while *deepseek-math-7b-rl* is further trained from it with reinforcement learning on GSM8K and MATH using the Group Relative Policy Optimization (GRPO) algorithm.
- **Mistral** (Chaplot, 2023; Wang et al., 2023): *mistral-7b-sft* is a supervised fine-tuned version of the Mistral-7B model on the MetaMATH dataset, while *math-shepherd-mistral-7b-rl* is further optimized from it using step-by-step Proximal Policy Optimization (PPO) guided by the MATH-SHEPHERD process reward model on GSM8K and MATH, leading to notable gains in mathematical reasoning accuracy.

Table 1: Comparison of four model pairs (SFT vs. RL) across three datasets, three evaluation metrics, and four hyperparameter settings. Missing values result from GPU memory overflow.

Dataset	Metric	Scale	Deepseek-Math		Mistral		Distilled-Qwen		Qwen2.5	
			α	SFT	+GRPO	SFT	+PPO	SFT	+GRPO	SFT
MATH	Act. Intens. ↑	0.03	2.29e-3	2.64e-3	9.47e-7	3.61e-6	6.18e-4	6.87e-4	1.11e-3	1.13e-3
		0.1	1.10e-3	1.31e-3	6.76e-4	7.71e-4	4.51e-4	5.59e-4	6.95e-4	6.90e-4
		0.3	7.47e-4	7.77e-4	4.49e-4	4.92e-4	-	-	4.39e-4	4.21e-4
		0.5	5.64e-4	6.02e-4	3.58e-4	4.05e-4	-	-	-	-
	Info. Complex. ↑	0.03	1.96e-1	2.01e-1	3.39e-2	1.58e-2	1.81e-1	2.30e-1	2.11e-1	1.74e-1
		0.1	1.72e-1	2.47e-1	1.41e-1	2.09e-1	1.11e-1	1.96e-1	1.60e-1	1.34e-1
		0.3	2.64e-1	4.11e-1	4.13e-2	2.86e-1	-	-	1.10e-1	1.34e-1
		0.5	2.71e-1	2.93e-1	4.52e-2	3.22e-1	-	-	-	-
	Dist. Kurt. ↓	0.03	3.93e+2	2.53e+2	4.22e+2	5.28e+2	6.78e+2	5.03e+2	3.96e+2	3.62e+2
		0.1	3.57e+2	2.23e+2	4.51e+2	3.07e+2	1.27e+3	9.20e+2	5.44e+2	4.83e+2
		0.3	3.11e+2	1.89e+2	3.35e+2	2.65e+2	-	-	8.49e+2	7.61e+2
		0.5	3.03e+2	1.89e+2	2.85e+2	2.20e+2	-	-	-	-
College Math	Act. Intens. ↑	0.03	2.36e-3	2.22e-3	1.77e-7	1.17e-6	7.08e-4	7.51e-4	1.20e-3	1.19e-3
		0.1	1.24e-3	1.21e-3	8.23e-4	9.06e-4	5.15e-4	5.76e-4	8.11e-4	8.10e-4
		0.3	7.61e-4	7.57e-4	4.92e-4	5.32e-4	-	-	4.76e-4	4.69e-4
		0.5	5.87e-4	5.99e-4	3.87e-4	4.47e-4	-	-	3.71e-4	3.53e-4
	Info. Complex. ↑	0.03	1.45e-1	1.96e-1	2.51e-2	1.14e-2	2.13e-1	2.35e-1	8.01e-2	2.17e-1
		0.1	2.08e-1	2.09e-1	1.65e-1	1.61e-1	1.32e-1	1.64e-1	1.34e-1	1.25e-1
		0.3	2.20e-1	2.89e-1	3.29e-1	2.88e-1	-	-	1.23e-1	9.95e-2
		0.5	2.53e-1	2.83e-1	2.68e-1	3.43e-1	-	-	1.11e-1	1.05e-1
	Dist. Kurt. ↓	0.03	4.71e+2	2.75e+2	4.81e+2	8.60e+2	5.86e+2	5.08e+2	4.57e+2	3.89e+2
		0.1	3.48e+2	2.88e+2	3.80e+2	2.64e+2	1.15e+3	8.88e+2	5.31e+2	4.60e+2
		0.3	3.31e+2	2.19e+2	2.77e+2	2.08e+2	-	-	7.51e+2	6.51e+2
		0.5	3.31e+2	2.12e+2	2.54e+2	2.22e+2	-	-	9.15e+2	7.48e+2
GSM8K	Act. Intens. ↑	0.03	3.08e-3	2.76e-3	4.83e-7	1.17e-6	1.06e-3	1.15e-3	2.13e-3	2.19e-3
		0.1	1.43e-3	1.50e-3	5.90e-4	6.59e-4	6.71e-4	7.72e-4	1.13e-3	1.13e-3
		0.3	7.80e-4	8.52e-4	3.86e-4	4.44e-4	-	-	6.46e-4	6.49e-4
		0.5	5.76e-4	6.52e-4	3.01e-4	3.60e-4	-	-	4.94e-4	4.90e-4
	Info. Complex. ↑	0.03	1.56e-1	1.56e-1	6.30e-2	4.00e-2	2.22e-1	3.33e-1	2.19e-1	2.53e-1
		0.1	1.50e-1	2.30e-1	8.43e-2	1.49e-1	1.60e-1	2.64e-1	1.64e-1	1.80e-1
		0.3	1.71e-1	2.27e-1	1.48e-1	2.09e-1	-	-	1.09e-1	1.57e-1
		0.5	1.37e-1	3.23e-1	1.69e-1	2.66e-1	-	-	1.14e-1	1.28e-1
	Dist. Kurt. ↓	0.03	4.73e+2	3.05e+2	2.05e+2	2.18e+2	3.81e+2	3.44e+2	4.68e+2	3.95e+2
		0.1	4.57e+2	2.79e+2	4.21e+2	3.07e+2	7.66e+2	5.60e+2	5.22e+2	4.53e+2
		0.3	3.85e+2	2.48e+2	3.99e+2	2.48e+2	-	-	7.17e+2	5.88e+2
		0.5	4.02e+2	2.49e+2	3.16e+2	2.18e+2	-	-	7.81e+2	6.73e+2

• **Distilled-Qwen** (Guo et al., 2025; Chen et al., 2025): *DeepSeek-R1-Distill-Qwen-7B* is a Qwen2.5-based model distilled from the larger DeepSeek-R1 reasoning model, trained via supervised distillation to inherit strong reasoning ability. In contrast, *AceReason-Nemotron-7B* starts from the same distilled checkpoint but is further optimized with reinforcement learning on curated math and code datasets using the GRPO algorithm, yielding significant gains in both mathematical and programming reasoning tasks.

• **Qwen2.5** (Qwen et al., 2025; Zhang et al., 2025a): *Qwen2.5-7B-SFT* is fine-tuned with supervised learning on the MATH and Numina-Math datasets, while *Qwen2.5-7B-DPO* is derived from that SFT model via iterative Direct Preference Optimization (DPO).

We conducted extensive analyses on three public mathematical benchmarks: *GSM8K*, *MATH*, and *College Math*. More detailed characteristics of the analyzed LLMs and implementation details are provided in the Appendix A and C. Thorough extensive evaluations on multiple benchmarks shown in Appendix D, the post-training generally improves the capability of different LLMs.

4.2 METRICS

In our experiments, we quantify differences in LLM behavior before and after reinforcement learning (RL) fine-tuning by analyzing the internal edge-weight matrices obtained from the graph-based

324 attribution procedure. Let $\mathbf{W}^{(k)} \in \mathbb{R}^{n_o \times n_i}$ denote the edge-weight matrix for sample k , with
 325 $k = 1, \dots, n$. The collection of all samples forms a tensor $\mathbf{W} \in \mathbb{R}^{n \times n_o \times n_i}$. Based on this input,
 326 we define three complementary metrics:
 327

328 **Activation Intensity (Act.Intens.).** This metric quantifies the average magnitude of all edge
 329 weights across every sample, output, and input, capturing both how many pathways in the LLM
 330 are activated and the strength of their activation:
 331

$$332 \text{Act.Intens.} = \frac{1}{n n_o n_i} \sum_{k=1}^n \sum_{o=1}^{n_o} \sum_{i=1}^{n_i} |W_{oi}^{(k)}|. \quad (14)$$

335 **Information Complexity (Info.Complex.).** To capture the heterogeneity and unpredictability of
 336 edge activations across the entire dataset, we compute a Shannon entropy over the absolute values
 337 of all edges from all samples, flattened into a single vector. Let p_b denote the normalized probability
 338 of bin b in a histogram of all $|W_{oi}^{(k)}|$ values, with B bins and a small constant ϵ to prevent $\log 0$:
 339

$$340 \text{Info.Complex.} = - \sum_{b=1}^B p_b \log(p_b + \epsilon). \quad (15)$$

343 Higher entropy values indicate more complex and less predictable distributions of edge activations,
 344 whereas lower values suggest concentrated or more regular patterns. This metric reflects the di-
 345 versity of active information pathways within the LLM during inference and highlights how RL
 346 fine-tuning may alter the overall internal information structure.
 347

348 **Distribution Kurtosis (Dist.Kurt.).** To quantify the overall shape and stability of edge-weight
 349 distributions, we first compute the kurtosis of each sample’s edge-weight matrix and then average
 350 across all samples:
 351

$$352 \text{Dist.Kurt.} = \frac{1}{n} \sum_{k=1}^n \left[\frac{\frac{1}{n_o n_i} \sum_{o,i} (W_{oi}^{(k)} - \mu^{(k)})^4}{\left(\frac{1}{n_o n_i} \sum_{o,i} (W_{oi}^{(k)} - \mu^{(k)})^2 \right)^2} - 3 \right], \quad (16)$$

356 where $\mu^{(k)}$ is the mean edge weight of sample k . Values approaching zero indicate that individ-
 357 ual edge-weight distributions approximate a normal distribution. Conversely, significant positive or
 358 negative values reflect leptokurtic (heavy-tailed) or platykurtic (light-tailed) distributions, respec-
 359 tively. This metric serves to evaluate the impact of RL fine-tuning on the tail behavior and outlier
 360 characteristics of the overall activation distribution.
 361

362 4.3 RESULTS AND ANALYSIS

363 Our main experimental results are presented in Table 1. We observe that the three model families,
 364 Deepseek-Math, Mistral, and Distilled-Qwen, exhibit largely consistent changes in the metrics be-
 365 fore and after RL fine-tuning. Specifically, Activation Intensity and Information Complexity tend to
 366 increase, while Distribution Kurtosis tends to decrease. Individual exceptions can be seen in some
 367 cases for Deepseek-Math and Mistral. However, as the scaling factor α controlling truncation length
 368 gradually increases, these exceptions diminish, and the observed patterns become largely consistent,
 369 indicating that the phenomenon is relatively robust. However, beyond these observations, we also
 370 find several differences in the experimental results of the Qwen2.5 series models trained with the
 371 DPO method. For instance, their activation strengths do not exhibit a clear increasing trend, and on
 372 the College Math dataset, as α grows to larger values, the Information Complexity metric of their
 373 internal pathways remains lower than that of the initial SFT model from which training began.
 374

375 Taken together, the above observations suggest two key conclusions: **(i)** Online RL fine-tuning for
 376 mathematical reasoning increases the extent and intensity of active information edges in the model.
 377 **(ii)** Online RL fine-tuning diversifies the activation patterns across these information pathways. We
 378 next provide further analyses to substantiate these conclusions.
 379

378
 379 **Pathway Engagement Induced by RL Fine-tuning.**
 380 As shown in our main results (Table 1), RL fine-
 381 tuning consistently increases Act.Intens. and decreases
 382 Dist.Kurt., meaning that a substantial number of low-
 383 activation edges become more active, effectively engag-
 384 ing a larger set of pathways. This trend is observed across
 385 different models, datasets, and hyperparameter settings.
 386 Figure 2 illustrates this effect with a representative case:
 387 the Mistral model on the MATH dataset at $\alpha = 0.5$. The
 388 relative change analysis highlights that many connections
 389 strengthen after PPO-based RL fine-tuning, confirming
 390 that reinforcement learning systematically enhances the
 391 propagation of internal signals.

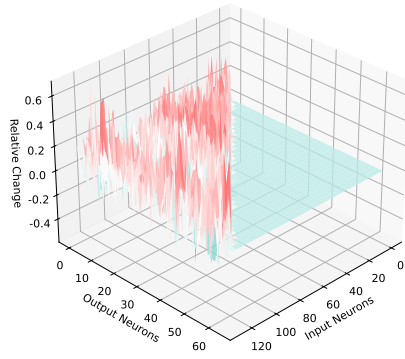
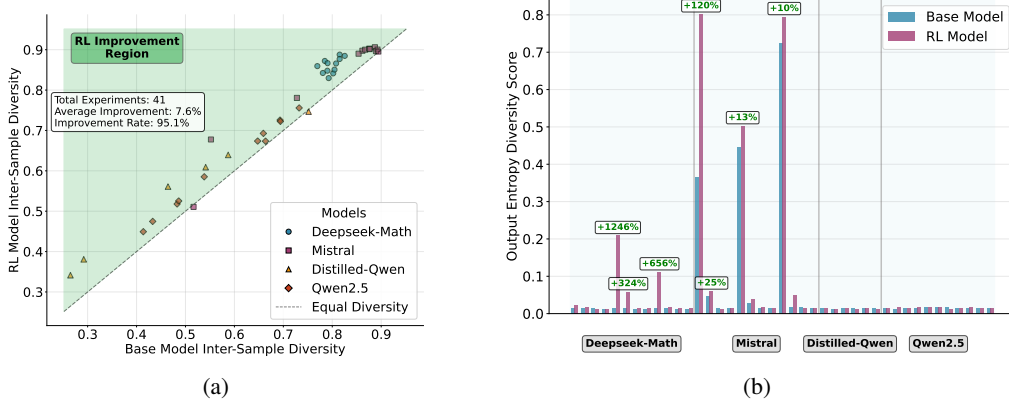


Figure 2: Relative change in edge activation strength after RL fine-tuning for the Mistral model on the MATH dataset with $\alpha = 0.5$.

392 **Diversity of Activation Patterns in Internal Repre-
 393 sentations.** In parallel, we find that Info.Complex. gen-
 394 erally increases and Dist.Kurt. decreases after RL fine-
 395 tuning as shown in Table 1, indicating that activation pat-
 396 terns become more diverse. We provide further visual-
 397 ization results relevant to this conclusion, as illustrated in
 398 Figure 3: panel (a) shows that across inference samples, the internal activation structures exhibit
 399 greater variability after RL, as quantified by an increase in one minus the mean correlation of edge-
 400 weight matrices between sample pairs, and panel (b) further demonstrates that output-edge entropy
 401 rises across most model–dataset–hyperparameter combinations. Together, these results indicate that
 402 RL enriches the connectivity structure of the internal circuitry, leading to more robust and flexible
 403 information flow essential for logical deduction. Furthermore, as shown in Figure 3, panel (a), the
 404 Qwen2.5 series models trained with the DPO algorithm also exhibit a certain degree of improve-
 405 ment in diversity. However, the magnitude of this improvement is relatively lower than that of
 406 models trained with other online RL methods.



407 Figure 3: Comparison before and after RL fine-tuning: (a) diversity of activation patterns across
 408 inference samples, including data from all datasets and α values; (b) entropy of output edge patterns
 409 per node. In (b), data points are arranged sequentially by dataset (College Math, GSM8K, MATH),
 410 iterating over $\alpha \in \{0.03, 0.1, 0.3, 0.5\}$ for each.

411 Based on Equation (4), we can interpret the observed phenomena by analyzing the fundamental
 412 differences in the support of the sampling distribution \mathcal{D} and the properties of the gradient coefficient
 413 $GC_{\mathcal{A}}$ across SFT, Online RL, and DPO.

414 For SFT, the data source is static, drawn from a fixed human-annotated distribution $\mathcal{D}_{SFT} =$
 415 $\{(q, o) \sim P_{\text{data}}\}$, with a constant gradient coefficient $GC_{SFT} = 1$. Consequently, the model opti-
 416 mizes its internal representations to minimize cross-entropy on a narrow, predefined manifold of
 417 “correct solutions.” This drives the model to converge towards a low-entropy mode that mimics the

432 training data, resulting in activations concentrated on a small number of outlier edges (high Distribution Kurtosis) and limited engagement of redundant pathways (low Activation Intensity).
 433

434 In contrast, Online RL algorithms like PPO and GRPO fundamentally alter the data source by introducing on-policy sampling, where outputs are dynamically generated by the evolving policy itself: $\mathcal{D}_{RL} = \{(q, \{o_i\}_{i=1}^G) \mid q \sim P_{data}, o_i \sim \pi_\theta(\cdot|q)\}$. This mechanism significantly expands the stochastic support set of the training distribution beyond the SFT subspace, providing the LLM with a richer set of reasoning path samples for each query q . Mechanistically, to handle the expanded state space encountered during exploration, the network is compelled to activate and reinforce latent or "dormant" internal circuits that were underutilized during SFT. Furthermore, the gradient coefficient in online RL varies dynamically based on feedback from the reward model or rule. Taking GRPO as an example, $GC_{GRPO} = \hat{A}_{i,t}(q, o, t, \pi_{rd}) + \beta \left(\frac{\pi_{ref}(o_{i,t}|o_{i,<t})}{\pi_\theta(o_{i,t}|o_{i,<t})} - 1 \right)$. To maximize expected reward, the model is driven to mobilize these less active internal circuits to master relatively "harder" problems, as correct responses to such instances typically yield significantly higher gradient coefficients. The observed increase in Activation Intensity and the simultaneous decrease in Distribution Kurtosis reflect this broader utilization of residual pathways. Moreover, as multiple distinct reasoning paths for the same question are reinforced, the entropy of the internal edge weight distribution increases.

449 Furthermore, from this unified perspective, we can elucidate why DPO exhibits distinct behaviors,
 450 particularly its failure to consistently enhance activation intensity and information complexity. Al-
 451 though DPO is mathematically derived from the RL objective, it operates as an offline (or semi-
 452 offline, where datasets are refreshed only periodically) algorithm. Its data source remains closer to a
 453 relatively more static distribution: $\mathcal{D}_{DPO} = \{(q, o^+, o^-) \sim P_{data}\}$, rather than the real-time policy
 454 π_θ . Since DPO restricts optimization to the fixed support set of an offline dataset and effectively
 455 retains only two potentially stale contrasting samples for each query q , the mechanistic pressure to
 456 expand the network's functional capacity through stochastic sampling is significantly weaker. This
 457 explains why Activation Intensity and Information Complexity do not show a consistent upward
 458 trend compared to the SFT baseline. However, DPO does successfully reduce Distribution Kur-
 459 tosis. This is because the preference optimization objective is driven by the gradient coefficient
 460 $GC_{DPO} = \sigma \left(\beta \log \frac{\pi_\theta(o^-|q)}{\pi_{ref}(o^-|q)} - \beta \log \frac{\pi_\theta(o^+|q)}{\pi_{ref}(o^+|q)} \right)$. This soft margin mechanism relaxes the strict
 461 token-matching constraints of SFT, favoring a broader reward maximization landscape and thereby
 462 inhibiting the emergence of high-intensity activation edges to some extent, which can be intuitively
 463 understood as mitigating rote memorization. Thus, while DPO attenuates the model's reliance on a
 464 few high-intensity edges during inference (low kurtosis), it lacks the on-policy exploration dynamics
 465 inherent to Online RL, which are essential for driving the systematic enhancement of average
 466 internal activation intensity and diversity.

467 In summary, we posit that the sampling process is the core factor driving the fundamental inter-
 468 internal differences between SFT, DPO, and various online-RL paradigms, which consequently leads to
 469 disparities in external performance. In Appendix B, we manipulated the sampling dynamics dur-
 470 ing online-RL by adjusting the training temperature and observed phenomena consistent with our
 471 expectations. These findings provide robust empirical support for our hypothesis.

472

473 5 RELATED WORKS

474

475 5.1 INTERPRETABILITY OF REINFORCEMENT LEARNING

477

478 The inherent opacity of deep reinforcement learning motivates studies on improving their explain-
 479 ability (Qing et al., 2022). Research in explainable RL can be generally categorized into pre-hoc
 480 and post-hoc techniques, where the former seeks to build inherently interpretable agents while the
 481 latter focuses on analyzing trained agents. Pre-hoc research direction focuses on creating inher-
 482 ently interpretable agents, such as neuro-symbolic systems that represent policies as mathematical
 483 expressions (Landajuela et al., 2021; Delfosse et al., 2023), ensuring transparency by design. On
 484 contrast, among post-hoc approaches, feature attribution methods are widely applied to generate
 485 saliency maps to highlight influential input features (Hao et al., 2022). Besides, another prominent
 486 post-hoc paradigm is policy distillation, where the behavior of a complex neural network is distilled
 487 into a simpler surrogate model, such as a decision tree, to provide a global summary of the agent's

486 strategy (Li et al., 2021). Furthermore, counterfactual methods provide an alternative explanatory
 487 lens by answering “what if” questions, identifying the minimal state alterations that would have led
 488 to a different action (Puri et al., 2019; Huber et al., 2023).

489 Collectively, these diverse approaches reflect a field moving from reactive explanation of opaque
 490 models towards transparent and trustworthy intelligent agents. However, these research mainly focus
 491 on lightweight RL agents for conventional decision-making tasks, while it remains unexplored how
 492 RL works in the emerging post-training applications, where LLMs are trained as the agent.

494 5.2 INTERPRETABILITY OF LARGE LANGUAGE MODELS

495 Research into the interpretability of LLMs has largely progressed along two complementary
 496 paradigms: mechanistic interpretability and representation interpretability (Singh et al., 2024).
 497 Mechanistic interpretability aims to reverse-engineer the patterns learned by a model by analyzing
 498 its fundamental components, such as neurons and attention heads, which often employs causal
 499 tracing techniques (Gantla, 2025). For instance, one study traced numerical hallucinations to a “Ben-
 500 ford’s Curse”, identifying a statistical bias learned from training data that was internalized by a small
 501 subset of feed-forward network (FFN) neurons, and then causally verified this by demonstrating that
 502 pruning these specific neurons corrected numerical errors (Shao et al., 2025). In contrast, rep-
 503 resentation interpretability mainly investigates what information is encoded in the model’s internal
 504 activation states via external probing models. A prominent line of work in this area uses lightweight
 505 probes varying from linear models (Kim et al., 2025) to graph models (Zheng et al., 2025), decoding
 506 concepts within the activation space of the model’s middle layers. These discovered representations
 507 are not merely correlational, but the learned probe weights can be repurposed as “steering vectors” to
 508 causally intervene on the activations during generation, thereby controlling the model’s output (Kim
 509 et al., 2025). While the former paradigm focuses on how a model computes, the latter reveals what
 510 knowledge it represents, together offering a more holistic understanding of these complex systems.

511 While such studies offer valuable perspectives on LLM interpretability, they predominantly focus
 512 on analyzing given LLMs without integrating the training methodology with which the LLMs are
 513 obtained into the investigation. In particular, it remains unclear how RL, the widely adopted tech-
 514 nique in post-training, is able to broadly enhance the capabilities of diverse LLMs with distinct
 515 architectural and functional characteristics.

516

571 6 CONCLUSIONS

591

592 We presented a systematic analysis of how reinforcement learning (RL) fine-tuning reshapes the
 593 internal circuitry of large language models (LLMs). Using edge attribution patching, we identified
 594 two robust effects across multiple model families: stronger average activation intensity and greater
 595 diversity in activation patterns. These findings suggest that online RL enhances both the redun-
 596 dancy and flexibility of information flow, which may underlie its superior generalization ability in
 597 mathematical domains. In contrast, DPO fine-tuning produced weaker or inconsistent changes, em-
 598 phasizing the methodological gap between static preference optimization and dynamic online RL.
 599 Our results provide a unified mechanistic perspective on RL post-training and offer guidance for the
 600 design of future post-training algorithms.

598

629

630 7 LIMITATIONS

631

632 Our study acknowledges certain limitations that outline important directions for future research.
 633 While the consistency of our results suggests potential broader applicability, our empirical vali-
 634 dation is currently confined to mathematical reasoning tasks. Verifying whether these internal cir-
 635 cuit dynamics hold in domains with open-ended outputs, such as code generation, creative writing,
 636 open-ended dialogue and so on, remains a critical subject for future investigation. We also note the
 637 limitation regarding model scale, as the significant memory overhead required for granular internal
 638 state analysis prevented us from extending our experiments to models larger than 7B parameters.
 639 Furthermore, concerning model architecture, although we endeavored to include a diverse range of
 640 open-source models, the current landscape is overwhelmingly dominated by the “LLaMA-style”
 641 structure.

540 ETHICS STATEMENT
541542 We fully use open-source models and datasets in the paper, which involve no problem regarding
543 privacy and copyright. We cite the resources in Section 4.1. This work does not involve human
544 subjects, discrimination, bias, or fairness concerns,
545546 REPRODUCIBILITY STATEMENT
547548 For Reproducibility, we describe the general experimental settings in Section 4.1, list the imple-
549 mentation details in Appendix C, and provide our anonymously open-sourced code at https://anonymous.4open.science/r/11m_rl_probing_analysis-F673.
550
551552 REFERENCES
553554 Josh Achiam, Steven Adler, Sandhini Agarwal, Lama Ahmad, Ilge Akkaya, Florencia Leoni Ale-
555 man, Diogo Almeida, Janko Altenschmidt, Sam Altman, Shyamal Anadkat, et al. Gpt-4 technical
556 report. *arXiv preprint arXiv:2303.08774*, 2023.
557558 Jinze Bai, Shuai Bai, Yunfei Chu, Zeyu Cui, Kai Dang, Xiaodong Deng, Yang Fan, Wenbin Ge,
559 Yu Han, Fei Huang, et al. Qwen technical report. *arXiv preprint arXiv:2309.16609*, 2023.
560561 Devendra Singh Chaplot. Albert q. jiang, alexandre sablayrolles, arthur mensch, chris bamford,
562 devendra singh chaplot, diego de las casas, florian bressand, gianna lengyel, guillaume lample,
563 lucile saulnier, lélio renard lavaud, marie-anne lachaux, pierre stock, teven le scao, thibaut lavril,
564 thomas wang, timothée lacroix, william el sayed. *arXiv preprint arXiv:2310.06825*, 3, 2023.
565566 Yang Chen, Zhuolin Yang, Zihan Liu, Chankyu Lee, Peng Xu, Mohammad Shoeybi, Bryan Catan-
567 zaro, and Wei Ping. Acereason-nemotron: Advancing math and code reasoning through rein-
568 forcement learning. *arXiv preprint arXiv:2505.16400*, 2025.
569570 Tianzhe Chu, Yuexiang Zhai, Jihan Yang, Shengbang Tong, Saining Xie, Dale Schuurmans, Quoc V
571 Le, Sergey Levine, and Yi Ma. Sft memorizes, rl generalizes: A comparative study of foundation
572 model post-training. *arXiv preprint arXiv:2501.17161*, 2025.
573574 Arthur Conmy, Augustine Mavor-Parker, Aengus Lynch, Stefan Heimersheim, and Adrià Garriga-
575 Alonso. Towards automated circuit discovery for mechanistic interpretability. *Advances in Neural
576 Information Processing Systems*, 36:16318–16352, 2023.
577578 Michael Han Daniel Han and Unsloth team. Unsloth, 2023. URL <http://github.com/unslothai/unsloth>.
579580 Quentin Delfosse, Hikaru Shindo, Devendra Dhami, and Kristian Kersting. Interpretable and ex-
581 plainable logical policies via neurally guided symbolic abstraction. *Advances in Neural Infor-
582 mation Processing Systems*, 36:50838–50858, 2023.
583584 Guanting Dong, Hongyi Yuan, Keming Lu, Chengpeng Li, Mingfeng Xue, Dayiheng Liu, Wei
585 Wang, Zheng Yuan, Chang Zhou, and Jingren Zhou. How abilities in large language models are
586 affected by supervised fine-tuning data composition. *arXiv preprint arXiv:2310.05492*, 2023.
587588 Sandeep Reddy Gantla. Exploring mechanistic interpretability in large language models: Chal-
589 lenges, approaches, and insights. In *2025 International Conference on Data Science, Agents &
590 Artificial Intelligence (ICDSAAI)*, pp. 1–8. IEEE, 2025.
591592 Daya Guo, Qihao Zhu, Dejian Yang, Zhenda Xie, Kai Dong, Wentao Zhang, Guanting Chen, Xiao
593 Bi, Yu Wu, YK Li, et al. Deepseek-coder: When the large language model meets programming—
594 the rise of code intelligence. *arXiv preprint arXiv:2401.14196*, 2024.
595596 Daya Guo, Dejian Yang, Haowei Zhang, Junxiao Song, Ruoyu Zhang, Runxin Xu, Qihao Zhu,
597 Shirong Ma, Peiyi Wang, Xiao Bi, et al. Deepseek-r1: Incentivizing reasoning capability in llms
598 via reinforcement learning. *arXiv preprint arXiv:2501.12948*, 2025.
599

594 Michael Hanna, Sandro Pezzelle, and Yonatan Belinkov. Have faith in faithfulness: Going beyond
 595 circuit overlap when finding model mechanisms. *arXiv preprint arXiv:2403.17806*, 2024.
 596

597 Qianyue Hao, Wenzhen Huang, Fengli Xu, Kun Tang, and Yong Li. Reinforcement learning en-
 598 hances the experts: Large-scale covid-19 vaccine allocation with multi-factor contact network. In
 599 *Proceedings of the 28th ACM SIGKDD conference on knowledge discovery and data mining*, pp.
 600 4684–4694, 2022.

601 Qianyue Hao, Lin Chen, Xiaoqian Qi, Yuan Yuan, Zefang Zong, Hongyi Chen, Keyu Zhao,
 602 Shengyuan Wang, Yunke Zhang, Jian Yuan, and Yong Li. Reinforcement learning in the era
 603 of large language models: Challenges and opportunities. *researchgate*, 2025.

604

605 Tobias Huber, Maximilian Demmler, Silvan Mertes, Matthew L Olson, and Elisabeth André.
 606 Ganterfactual-rl: Understanding reinforcement learning agents’ strategies through visual coun-
 607 terfactual explanations. *arXiv preprint arXiv:2302.12689*, 2023.

608 Junsol Kim, James Evans, and Aaron Schein. Linear representations of political perspective emerge
 609 in large language models. *arXiv preprint arXiv:2503.02080*, 2025.

610

611 Komal Kumar, Tajamul Ashraf, Omkar Thawakar, Rao Muhammad Anwer, Hisham Cholakkal,
 612 Mubarak Shah, Ming-Hsuan Yang, Phillip HS Torr, Fahad Shahbaz Khan, and Salman Khan.
 613 Llm post-training: A deep dive into reasoning large language models. *arXiv preprint
 614 arXiv:2502.21321*, 2025.

615 Mikel Landajuela, Brenden K Petersen, Sookyoung Kim, Claudio P Santiago, Ruben Glatt, Nathan
 616 Mundhenk, Jacob F Pettit, and Daniel Faissol. Discovering symbolic policies with deep rein-
 617 forcement learning. In *International Conference on Machine Learning*, pp. 5979–5989. PMLR,
 618 2021.

619

620 Zhao-Hua Li, Yang Yu, Yingfeng Chen, Ke Chen, Zhipeng Hu, and Changjie Fan. Neural-to-tree
 621 policy distillation with policy improvement criterion. *arXiv preprint arXiv:2108.06898*, 2021.

622

623 Jianxing Liao, Tian Zhang, Xiao Feng, Yusong Zhang, Rui Yang, Haorui Wang, Bosi Wen, Ziying
 624 Wang, and Runzhi Shi. Rlmr: Reinforcement learning with mixed rewards for creative writing.
 625 *arXiv preprint arXiv:2508.18642*, 2025.

626

627 Hunter Lightman, Vineet Kosaraju, Yuri Burda, Harrison Edwards, Bowen Baker, Teddy Lee, Jan
 628 Leike, John Schulman, Ilya Sutskever, and Karl Cobbe. Let’s verify step by step. In *The Twelfth
 629 International Conference on Learning Representations*, 2023.

630

631 Aixin Liu, Bei Feng, Bing Xue, Bingxuan Wang, Bochao Wu, Chengda Lu, Chenggang Zhao,
 632 Chengqi Deng, Chenyu Zhang, Chong Ruan, et al. Deepseek-v3 technical report. *arXiv preprint
 633 arXiv:2412.19437*, 2024.

634

635 Jijia Liu, Feng Gao, Bingwen Wei, Xinlei Chen, Qingmin Liao, Yi Wu, Chao Yu, and Yu Wang.
 636 What can rl bring to vla generalization? an empirical study. *arXiv preprint arXiv:2505.19789*,
 637 2025.

638

639 Chengqi Lyu, Songyang Gao, Yuzhe Gu, Wenwei Zhang, Jianfei Gao, Kuikun Liu, Ziyi Wang,
 640 Shuaibin Li, Qian Zhao, Haian Huang, et al. Exploring the limit of outcome reward for learning
 641 mathematical reasoning. *arXiv preprint arXiv:2502.06781*, 2025.

642

643 Neel Nanda. Attribution patching: Activation patching at industrial scale. *URL: https://www.neel-
 644 nanda.io/mechanistic-interpretability/attribution-patching*, 2023.

645

646 Nikaash Puri, Sukriti Verma, Piyush Gupta, Dhruv Kayastha, Shripad Deshmukh, Balaji Krishna-
 647 murthy, and Sameer Singh. Explain your move: Understanding agent actions using specific and
 648 relevant feature attribution. *arXiv preprint arXiv:1912.12191*, 2019.

649

650 Yunpeng Qing, Shunyu Liu, Jie Song, Huiqiong Wang, and Mingli Song. A survey on explain-
 651 able reinforcement learning: Concepts, algorithms, challenges. *arXiv preprint arXiv:2211.06665*,
 652 2022.

648 Qwen, :, An Yang, Baosong Yang, Beichen Zhang, Binyuan Hui, Bo Zheng, Bowen Yu, Chengyuan
 649 Li, Dayiheng Liu, Fei Huang, Haoran Wei, Huan Lin, Jian Yang, Jianhong Tu, Jianwei Zhang,
 650 Jianxin Yang, Jiaxi Yang, Jingren Zhou, Junyang Lin, Kai Dang, Keming Lu, Keqin Bao, Kexin
 651 Yang, Le Yu, Mei Li, Mingfeng Xue, Pei Zhang, Qin Zhu, Rui Men, Runji Lin, Tianhao Li,
 652 Tianyi Tang, Tingyu Xia, Xingzhang Ren, Xuancheng Ren, Yang Fan, Yang Su, Yichang Zhang,
 653 Yu Wan, Yuqiong Liu, Zeyu Cui, Zhenru Zhang, and Zihan Qiu. Qwen2.5 technical report, 2025.
 654 URL <https://arxiv.org/abs/2412.15115>.

655 Yi Ren and Danica J Sutherland. Learning dynamics of llm finetuning. *arXiv preprint*
 656 *arXiv:2407.10490*, 2024.

657 John Schulman, Filip Wolski, Prafulla Dhariwal, Alec Radford, and Oleg Klimov. Proximal policy
 658 optimization algorithms. *arXiv preprint arXiv:1707.06347*, 2017.

659 Jiandong Shao, Yao Lu, and Jianfei Yang. Benford’s curse: Tracing digit bias to numerical hallucin-
 660 nation in llms. *arXiv preprint arXiv:2506.01734*, 2025.

661 Zhihong Shao, Peiyi Wang, Qihao Zhu, Runxin Xu, Junxiao Song, Xiao Bi, Haowei Zhang,
 662 Mingchuan Zhang, YK Li, Yang Wu, et al. Deepseekmath: Pushing the limits of mathemati-
 663 cal reasoning in open language models. *arXiv preprint arXiv:2402.03300*, 2024.

664 Chandan Singh, Jeevana Priya Inala, Michel Galley, Rich Caruana, and Jianfeng Gao. Rethinking
 665 interpretability in the era of large language models. *arXiv preprint arXiv:2402.01761*, 2024.

666 Aaquib Syed, Can Rager, and Arthur Conmy. Attribution patching outperforms automated circuit
 667 discovery. *arXiv preprint arXiv:2310.10348*, 2023.

668 Ashish Vaswani, Noam Shazeer, Niki Parmar, Jakob Uszkoreit, Llion Jones, Aidan N Gomez,
 669 Łukasz Kaiser, and Illia Polosukhin. Attention is all you need. *Advances in neural informa-
 670 tion processing systems*, 30, 2017.

671 Peiyi Wang, Lei Li, Zhihong Shao, RX Xu, Damai Dai, Yifei Li, Deli Chen, Yu Wu, and Zhifang
 672 Sui. Math-shepherd: Verify and reinforce llms step-by-step without human annotations. *arXiv*
 673 *preprint arXiv:2312.08935*, 2023.

674 Fengli Xu, Qianyue Hao, Zefang Zong, Jingwei Wang, Yunke Zhang, Jingyi Wang, Xiaochong Lan,
 675 Jiahui Gong, Tianjian Ouyang, Fanjin Meng, et al. Towards large reasoning models: A survey of
 676 reinforced reasoning with large language models. *arXiv preprint arXiv:2501.09686*, 2025.

677 Shusheng Xu, Wei Fu, Jiaxuan Gao, Wenjie Ye, Weilin Liu, Zhiyu Mei, Guangju Wang, Chao Yu,
 678 and Yi Wu. Is dpo superior to ppo for llm alignment? a comprehensive study. *arXiv preprint*
 679 *arXiv:2404.10719*, 2024.

680 Qiyi Yu, Zheng Zhang, Ruofei Zhu, Yufeng Yuan, Xiaochen Zuo, Yu Yue, Weinan Dai, Tiantian
 681 Fan, Gaohong Liu, Lingjun Liu, et al. Dapo: An open-source llm reinforcement learning system
 682 at scale. *arXiv preprint arXiv:2503.14476*, 2025.

683 Lifan Yuan, Wendi Li, Huayu Chen, Ganqu Cui, Ning Ding, Kaiyan Zhang, Bowen Zhou,
 684 Zhiyuan Liu, and Hao Peng. Free process rewards without process labels. *arXiv preprint*
 685 *arXiv:2412.01981*, 2024.

686 Hanning Zhang, Jiarui Yao, Chenlu Ye, Wei Xiong, and Tong Zhang. Online-dpo-r1: Unlocking
 687 effective reasoning without the ppo overhead, 2025. *Notion Blog*, 2025a.

688 Kaiyan Zhang, Yuxin Zuo, Bingxiang He, Youbang Sun, Runze Liu, Che Jiang, Yuchen Fan, Kai
 689 Tian, Guoli Jia, Pengfei Li, et al. A survey of reinforcement learning for large reasoning models.
 690 *arXiv preprint arXiv:2509.08827*, 2025b.

691 Yu Zheng, Yuan Yuan, Yong Li, and Paolo Santi. Probing neural topology of large language models.
 692 *arXiv preprint arXiv:2506.01042*, 2025.

693

694

695

696

697

698

699

700

701

702 A CHARACTERISTICS OF ANALYZED LLMs

704 We employed four pairs of large language models (LLMs), each consisting of a base model (SFT)
 705 and its post-trained RL counterpart. The models and their download links are listed below:
 706

707 • **DeepSeek-Math**

708 – `deepseek-math-7b-instruct`: <https://huggingface.co/deepseek-ai/deepseek-math-7b-instruct>
 709 – `deepseek-math-7b-rl`: <https://huggingface.co/deepseek-ai/deepseek-math-7b-rl>

710 • **Mistral**

711 – `mistral-7b-sft`: <https://huggingface.co/peiyi9979/mistral-7b-sft>
 712 – `math-shepherd-mistral-7b-rl`: <https://huggingface.co/peiyi9979/math-shepherd-mistral-7b-rl>

713 • **Distilled-Qwen**

714 – `DeepSeek-R1-Distill-Qwen-7B`: <https://huggingface.co/deepseek-ai/DeepSeek-R1-Distill-Qwen-7B>
 715 – `AceReason-Nemotron-7B`: <https://huggingface.co/nvidia/AceReason-Nemotron-7B>

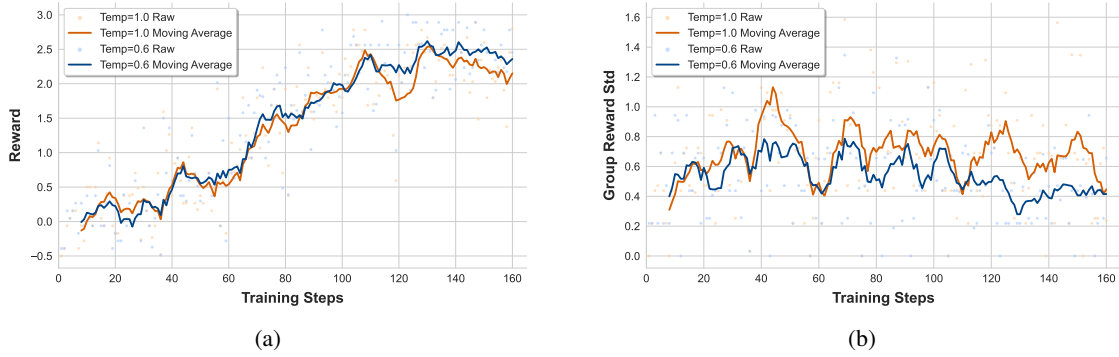
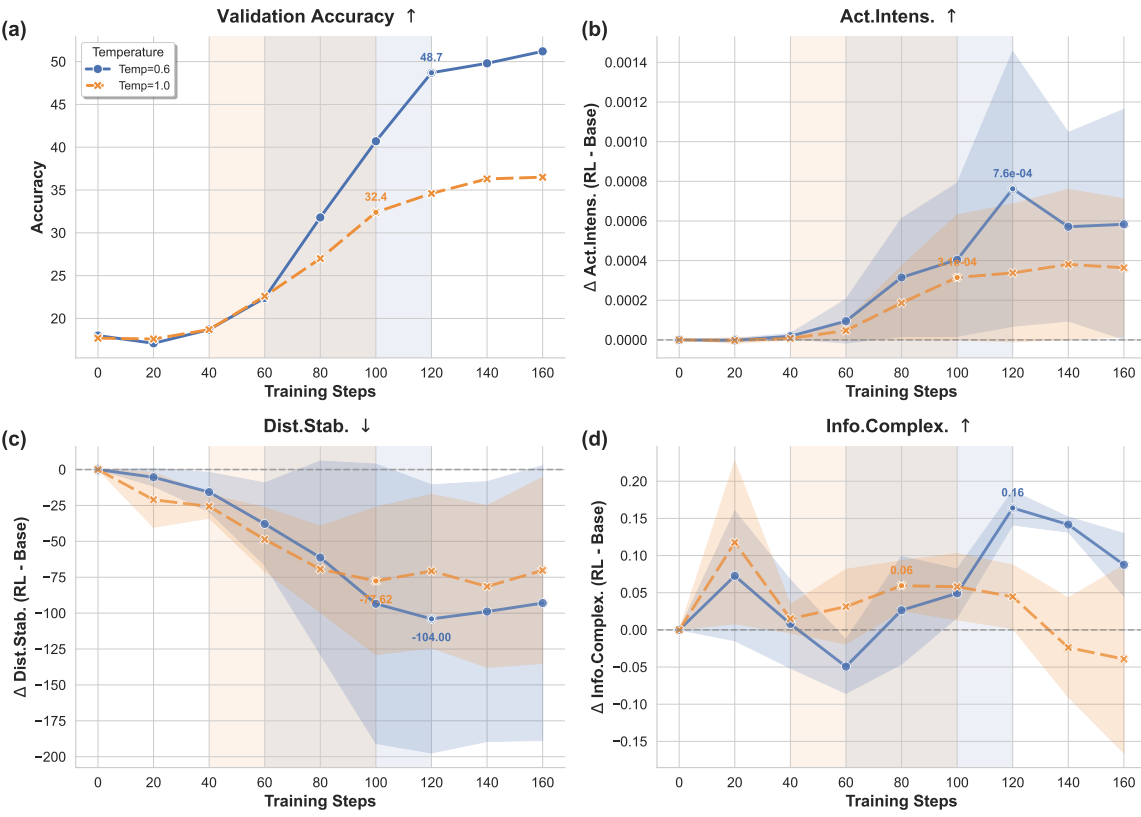
716 • **Qwen2.5**

717 – `Qwen2.5-7B-SFT`: <https://huggingface.co/RLHFlow/Qwen2.5-7B-SFT>
 718 – `Qwen2.5-7B-DPO`: <https://huggingface.co/RLHFlow/Qwen2.5-7B-DPO>

719 As summarized in Table 2, these LLMs are designed with distinctive structural and functional characteristics.
 720

721 Table 2: Structural and functional characteristics of the analyzed LLMs.

722 LLM series	723 Parameter size	724 # layers	725 # heads	726 Max ctx	727 Dim	728 Vocab size
729 DeepSeek-Math	730 7B	731 30	732 32	733 4096	734 4096	735 102400
736 Mistral	737 7B	738 32	739 32	740 4096	741 4096	742 32000
743 Distilled-Qwen	744 7B	745 28	746 28	747 131072	748 3584	749 152064
750 Qwen-2.5	751 7B	752 28	753 28	754 8192	755 3584	756 151665

756 **B TRAINING DYNAMICS UNDER SAMPLING INTERVENTIONS**
757759
760
761
762
763
764
765
766
767
768
769
770
771 **Figure 4: Smoothed moving-average curves of reward and group reward standard deviation during**
772 **RL training under different temperatures, with a sliding window length of 8.**801 **Figure 5: (a) Accuracy of models trained with different numbers of RL steps on the GSM8K test**
802 **set. (b), (c), and (d) show, respectively, the differences in Activation Intensity, Distribution Stability,**
803 **and Information Complexity between models trained with different numbers of RL steps and the**
804 **initial model. We highlight the training intervals where the performance gains are most pronounced**
805 **for temperature = 0.6 and temperature = 1.0, corresponding to [60, 120] and [40, 100], and mark the**
806 **extrema of each metric within these intervals in the expected direction.**807
808

To investigate whether the observed internal circuit changes are causal drivers of performance improvement rather than mere byproducts, we designed an intervention experiment. These changes

809

specifically refer to the increased activation intensity and the enhancement of pattern diversity. We

810 employed Qwen2.5-3B-Instruct¹ (Daniel Han & team, 2023) as the base model and limited its maximum generation length to 200 tokens to constrain its initial reasoning capabilities. On this basis, 811 we conducted reinforcement learning training on the GSM8K training set using an improved variant 812 of the GRPO algorithm (Yu et al., 2025). The experiment was configured with a batch size of 32 813 and sampled 4 candidate responses per query. We utilized the RLVR reward function where correct 814 answers received 3 points and completely incorrect answers received -0.5 points. Partial correctness 815 was scored proportionally based on the deviation between the prediction and the ground truth. 816

817 Our core hypothesis asserts that effective on-policy exploration drives the activation and consolidation 818 of beneficial internal circuits and subsequently leads to performance gains. To verify this, 819 we required a control variable to modulate exploration quality. We selected sampling temperature 820 as the intervention method because excessively high temperatures theoretically introduce excessive 821 randomness and alter sampling effectiveness. We compared two temperature settings. A temperature 822 of 0.6 represents effective exploration under standard settings while 1.0 represents noisy exploration 823 under high-entropy settings.

824 Figure 4 illustrates the reward trajectories and the standard deviation of the Group Reward during 825 training. As shown in Figure 4(b), the Group Reward standard deviation under the 1.0 temperature 826 setting is significantly higher than that of the 0.6 setting. This confirms that high temperatures induce 827 higher output mode variability (Liu et al., 2025; Ren & Sutherland, 2024). Such excessive variance 828 implies that the signals generated during exploration are noisier. Consequently, it becomes difficult 829 for the model to reliably identify the underlying patterns corresponding to correct solutions.

830 We tracked the evolution of three key internal metrics relative to the initial SFT model as detailed 831 in Figure 5(b)-(d). We observed significant differences during the critical mid-training phase be- 832 tween steps 40 and 120. At temperature 0.6, activation intensity showed a clear increasing trend 833 and peaked around step 120. In contrast, the growth of this metric was significantly suppressed at 834 temperature 1.0 where the peak was markedly lower than that of the low-temperature group. This 835 suggests that noisy sampling hindered the full activation of latent dormant circuits. Similarly, the 836 information complexity for the 0.6 group rose sharply between steps 100 and 120. Conversely, the 837 1.0 group failed to sustain growth and even exhibited a decline during mid-training. Regarding 838 distribution kurtosis in Figure 5(c), the 0.6 group showed a significant decrease. This implies that 839 the model no longer relies excessively on a few concentrated high-activation pathways for reason- 840 ing. In comparison, the 1.0 group exhibited a smaller decrease. Overall, the 0.6 temperature group 841 achieved higher peaks in activation intensity and information complexity alongside lower valleys in 842 distribution kurtosis compared to the 1.0 group during the mid-training phase.

843 The differences in internal circuits mapped directly to downstream task performance. Figure 5(a) 844 illustrates the changes in GSM8K test accuracy. The accuracy of the 0.6 group climbed rapidly 845 alongside the expected changes in internal metrics and finally reached 51.2%. Conversely, the 846 performance growth of the 1.0 group was slow due to suppressed internal circuit evolution and 847 eventually stagnated around 36.5%. This is far below the control group. The results indicate that 848 performance gains are substantially weakened when the normal evolution of internal circuits is 849 artificially suppressed via high-temperature sampling. This intervention-suppression effect provides 850 effective empirical support for our causal hypothesis. This provides empirical support for the view 851 that diverse and high-intensity internal pathway activation is a key mechanism bridging effective 852 sampling and performance improvement, rather than being a simple byproduct.

853
854
855
856
857
858
859
860
861
862
863

¹<https://huggingface.co/unsloth/Qwen2.5-3B-Instruct>

864
865
C IMPLEMENTATION DETAILS866
867 In this section, we provide all implementation details for reproducibility in Table 3. In the experi-
868
869
870
871
872
873
874
875
876
877
878
879
880
881
882
883
884
885
886
887
888
889
890
891
892
893
894
895
896
897
898
899
900
901
902
903
904
905
906
907
908
909
910
911
912
913
914
915
916
917

Table 3: Implementation details

Module	Element	Detail
System	OS	Ubuntu 22.04.3 LTS
	CUDA	12.2
	Python	3.11
	Pytorch	2.7.0+cu26
	Device	2*NVIDIA A100 80G

918 D PERFORMANCE OF LLMs
919920 Here we compare the performance of LLMs before and after post-training on multiple benchmarks.
921 As shown in Table 4, post-training generally improves the capability of different LLMs.
922923 Table 4: Performance comparisons of LLMs before and after post-training. Bold numbers indicate
924 better performance.
925

926 LLM series	927 Post-training	928 MATH	929 GSM8K	930 Minerva math	931 Olympiad bench	932 College math	933 AIME24	934 AMC23
929 DeepSeek-Math	Before	46.2	82.1	22.1	14.5	30.8	3.3	17.5
	After	52.6	87.9	27.2	18.2	33.5	6.7	25.0
931 Mistral	Before	29.1	78.2	12.1	5.5	17.5	0.0	12.5
	After	32.6	84.2	11.8	9.2	19.9	0.0	12.5
933 DS-Distill-Qwen	Before	88.4	90.3	43.0	49.8	40.0	46.7	87.5
	After	95.4	93.4	55.9	65.9	44.6	70.0	95.0
935 Qwen-2.5	Before	75.7	92.2	32.7	37.6	41.9	16.7	62.5
	After	82.6	92.0	40.1	46.4	42.5	26.7	67.5

937
938
939
940
941
942
943
944
945
946
947
948
949
950
951
952
953
954
955
956
957
958
959
960
961
962
963
964
965
966
967
968
969
970
971

972 E USE OF LLMs
973974 The authors used LLMs to aid or polish paper writing, but all content has been carefully reviewed
975 by the author. The authors used LLMs for literature retrieval and discovery, but all related works
976 have been carefully reviewed and organized by the author. The research ideation in this work was
977 entirely completed by the author and does not involve the use of LLMs.
978
979
980
981
982
983
984
985
986
987
988
989
990
991
992
993
994
995
996
997
998
999
1000
1001
1002
1003
1004
1005
1006
1007
1008
1009
1010
1011
1012
1013
1014
1015
1016
1017
1018
1019
1020
1021
1022
1023
1024
1025